Double layer effects in laser-ablation plasma plumes

Nadezhda M. Bulgakova, Alexander V. Bulgakov, and Oleg F. Bobrenok
Institute of Thermophysics, Lavrentyev Prospect 1, 630090 Novosibirsk, Russia
(Received 2 August 1999; revised manuscript received 13 June 2000)

Charge-collector probe measurements have been performed to elucidate ion acceleration in laser-induced plasma plumes over a range of laser fluences important for pulsed laser deposition. The fundamental (1064 nm) or second (532 nm) harmonics of a Nd:YAG laser were used for ablation. The evolution of the time-of-flight ion signal from single-peaked to double-peaked and again to single-peaked with increasing laser fluence in the range of 2–25 J/cm^2 has been followed. The analysis of the ion velocity distributions shows that increasing laser fluence results in the appearance of a portion of accelerated ions that can be recognized as an additional fast peak in the time-of-flight distribution. The dependencies of the ion signal on the target-to-collector distance, the background pressure, and the wavelength of laser radiation have been studied. The results are discussed from the viewpoint of the generation of a self-consistent ambipolar electric field (so-called double layer). The observed ion acceleration suggests that formation in the plume of a high-energetic electron tail due to absorption of laser radiation is responsible for the development of a double layer.

PACS number(s): 52.50.Jm, 79.20.Ds, 81.15.Fg

I. INTRODUCTION

The subject of this paper is ion acceleration in a laser-induced plasma plume under ablation conditions used typically for deposition of thin films. The phenomenon of ion acceleration in a plasma expanding into vacuum or low-density background gas has long been known for laser-produced plasmas, vacuum arcs, space plasmas, etc. Plyutto [1] was the first to propose a self-consistent ambipolar electric field arising in the expanding plasma (the so-called double layer) as a possible mechanism responsible for this phenomenon. A comprehensive study of the double layer (DL) formation has been presented in Ref. [2] where a detailed picture of the ion dynamics and electric field evolution during plasma expansion were obtained. The typical characteristics of the DL are presented in Fig. 1. The double layer is formed as a result of the spatial charge separation in the expanding plasma [Fig. 1(a)]. The electric potential [Fig. 1(b)] and electric field [Fig. 1(c)] arise as a consequence of the breaking of quasineutrality. The ions, which enter the region of the potential drop, experience acceleration. In essence, the DL divides the expanding plasma into regions with thermal and accelerated ions.

In numerous charge-collector probe measurements of ion emission from a high-temperature laser-produced plasma, double-peaked signals were obtained, suggesting that the ions were divided into fast and thermal components [3–5]. Other observations indicate that multipeak structure can arise, especially for the differently charged ions [6–8]. Whether single peak or multipeak structures are observed, ion acceleration is an integral part of the laser-produced plasma experiments. The fast ions can carry greater energy than the thermal expansion energy of the plasma [6,7,9] and they are confined within a narrow angle to the target normal [6,10].

The above-mentioned investigations relate to high-power laser irradiance inherent in laser fusion experiments. In recent years, laser ablation at moderate fluences (1–10 J/cm^2) has taken on a new significance due to its use in pulsed laser deposition (PLD) of thin solid films. Splitting of the ion flux into two or several components under PLD conditions has also been observed [11–16]. Although the fractional ionization of the particles arriving at the substrate is relatively low (typically ~1% or less [17]), fast ions are found to play an important role in the deposition process [18–23]. As in the high fluence experiments, ion acceleration is related to the ambipolar electric field [15] and the concept of the DL is invoked [24,25]. However, the physical processes responsible for the formation of the ion velocity distribution during PLD, specifically, the contribution of the DL, are not fully understood. The nature of the double-peaked ion signal was explained in Refs. [11,12] by the effect of background gas. On the other hand, judging from works [13–15], ion flux splitting seems to be more general phenomenon which manifests itself for ablation in vacuum as well.

Ion acceleration during laser plasma expansion has become the topic of a large body of theoretical research. Most of the theoretical treatments have studied collisionless plasmas on the basis of the hydrodynamic equations together with Poisson's equation when the electron temperature remains constant during expansion. For semi-infinite plasmas

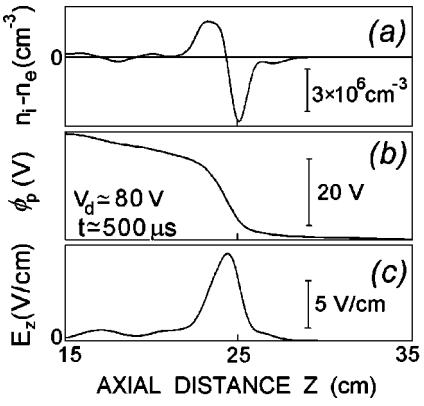

FIG. 1. Example of space charge separation (a), electric potential (b) and electric field (c) profiles across the double layer, adopted from Hairapetian and Stenzel [2].

considered in the frames of single-electron-temperature (SET) fluid theory, the ion front has been found to be accelerated to velocities comparable with the electron velocities, but the acceleration takes place within a thin layer in the plume periphery where quasineutrality of the plasma is broken down [26–28]. Bezzerides *et al.* [29] have deduced that, in an expanding two-electron-temperature (TET) plasma, a rarefaction shock wave may be formed, which conceptually represents a DL structure. The formation of such a shock wave is determined by the ratios of hot- to cold-electron temperatures (T_h/T_c) and densities (n_h/n_c). According to the model [30], the T_h/T_c and n_h/n_c values for the laser-produced plasma can be determined from experimental ion velocity spectra. It was shown that an external energy source, e.g., absorption of laser radiation, is essential to maintain the TET distribution during plasma expansion [31,32].

The theoretical studies demonstrate rather contradictory results with respect to the electron energy distribution responsible for ion acceleration. The majority of approaches indicate that the hot electron population is critical for producing the DL in the expanding plasma and thus for obtaining a pronounced ion acceleration [29–34]. On the other hand, a narrow region with a sharp increase in the ambipolar electric field (typical DL [2]) is also found for SET plasma [26–28]. In the letter case, the DL is formed in the plasma boundary whereas for a TET distribution it appears between the cold electrons and the accelerated ions. Furthermore, calculations based on the ion Vlasov equation revealed the development of the DL regardless of the electron energy distribution with a possibility to obtain a twin DL structure for a TET plasma [35].

Theoretical understanding of DL formation in an expanding plasma has fallen short of generation a clear picture of ion acceleration under PLD conditions. Analytical and numerical models listed above have two common features. All of them are collisionless and one dimensional. In real situations, when pulsed laser radiation (powerful or moderate) evaporates a flat solid target, a simple estimation shows that plasma cannot be considered as collisionless in the one-dimensional expansion stage [36,37]. In such a plasma, the degree of ionization decreases during expansion due to recombination processes. As a result, the ambipolar electric field responsible for ion acceleration apparently varies in a much greater range than it can be described in the framework of a collisionless model.

In this work, charge-collector probe measurements have been performed to elucidate ion acceleration in laser-produced carbon plasmas over a fluence range typical for PLD of diamondlike films [20,21]. The evolution of the ion signal from single-peaked to double-peaked and back again to single-peaked with increasing fluence has been followed for the case of a plasma expanding in vacuum. The dependencies of the time-of flight (TOF) ion signal on laser fluence, target-to-collector distance, background gas pressure, and wavelength of laser radiation, have been studied. The results are analyzed from the viewpoint of DL formation.

II. EXPERIMENTAL

The experiments were carried out in a 145-mm-diameter vacuum chamber evacuated to a base pressure of 10^{-3} Pa. In order to examine the effect of ambient gas on the plasma expansion, the air pressure was varied in the range of 0.1–100 Pa (see Sec. III E). A Q-switched Nd:YAG laser (13 ns FWHM pulse) operated either at the fundamental (1064 nm) or the second (532 nm) harmonic was used to ablate a molded graphite target (99.99% purity, 1.87 g/cm^3 density). After passing an aperture, the laser pulse was focused by a 35 cm focal length lens on a target surface at 20° incidence angle (as measured from the target normal). Laser fluences on the target in the range of 3–25 J/cm^2 (at 1064 nm) and 2–7 J/cm^2 (at 532 nm) could be obtained by varying the operating parameters of the laser. The spot size was measured using optical microscope analysis of the irradiated area after a large number of pulses. A circular mask of 2.5 mm in diameter was used to form the beam in front of the lens and to cut off the inhomogeneous edges of the laser beam. The target was placed a little beyond the focus of the lens to obtain a uniform laser energy distribution within the irradiated area.

The TOF spectra of laser-produced positive ions were studied using the ion probe technique. The ion probe consisted of a 12 mm square plate collector and a pair of high transmittance grids in front of it. Both collector and grids were maintained at suitable potentials in order to provide rejection of the electrons of the laser-generated plasma and to overcome secondary electron emission [9,38,39]. The first shielding grid was grounded, as was the target. The bias negative voltage of the collector was fixed at -110 V. The second grid was kept at -30 V with respect to the collector to prevent secondary electrons from leaving the collector [9,39]. The ion signals were recorded on a fast oscilloscope (HP54610B, 500 MHz bandwidth), across a 50 Ω terminator, and stored in a PC.

Experiments were performed for two target-to-collector distances, namely, 30 and 89 mm. The ion probe was placed along the target normal and oriented parallel to the target surface. The TOF spectra have been obtained for plasmas generated from the etched graphite surface, that is, from regions previously irradiated with a fairly large number of laser pulses. The target could be translated during measurements to avoid deep cratering. Such irradiation conditions appear to be more typical for PLD applications as compared with ablation of a fresh surface [40]. In order to determine the ablation rate per pulse, the weight of the target was measured before and after irradiation.

III. RESULTS AND DISCUSSION

A. Ablation in vacuum at 1064 nm

Figure 2 shows typical TOF ion signals for different laser fluences at 1064-nm wavelength for a target-to-collector distance of 30 mm. At low laser fluence (F_0) up to approximately 9 J/cm^2, the ion probe signal represents a single peak. As laser fluence increases, an additional fast peak arises with an earlier arrival time which is small compared to the slow one at $F_0 < 12$ J/cm^2. The TOF spectra behave as if the ions transfer gradually from the slow to fast peak with increasing laser fluence (see curves for 10, 12, and 13 J/cm^2, sequentially). As a result, at $F_0 = 14$ J/cm^2 the slow peak is weak in relation to the fast component. At higher laser flu-

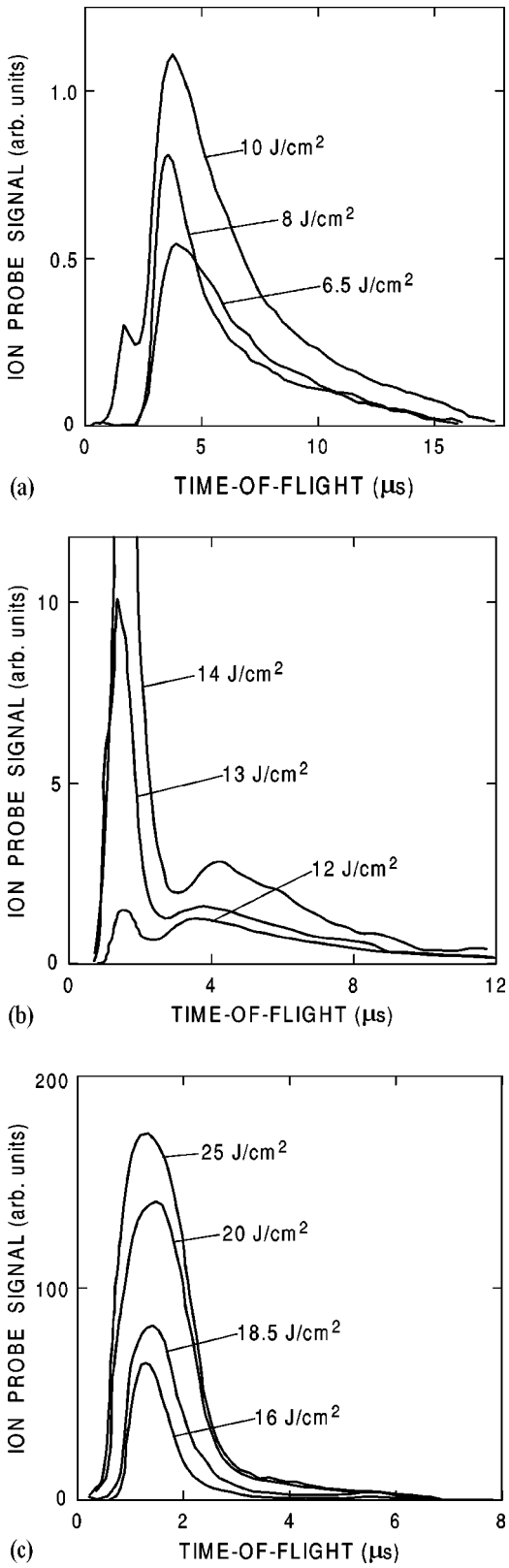

FIG. 2. Time-of-flight (TOF) distributions of carbon ions produced in vacuum by 1064-nm laser radiation at different fluences. The target-to-collector distance is 30 mm.

ences the ion flux is again single peaked since the slow peak disappears against the background of the fast ion signal [Fig. 2(c)].

As the target-to-collector distance increases, the TOF distribution changes. The transformation of the ion signal with

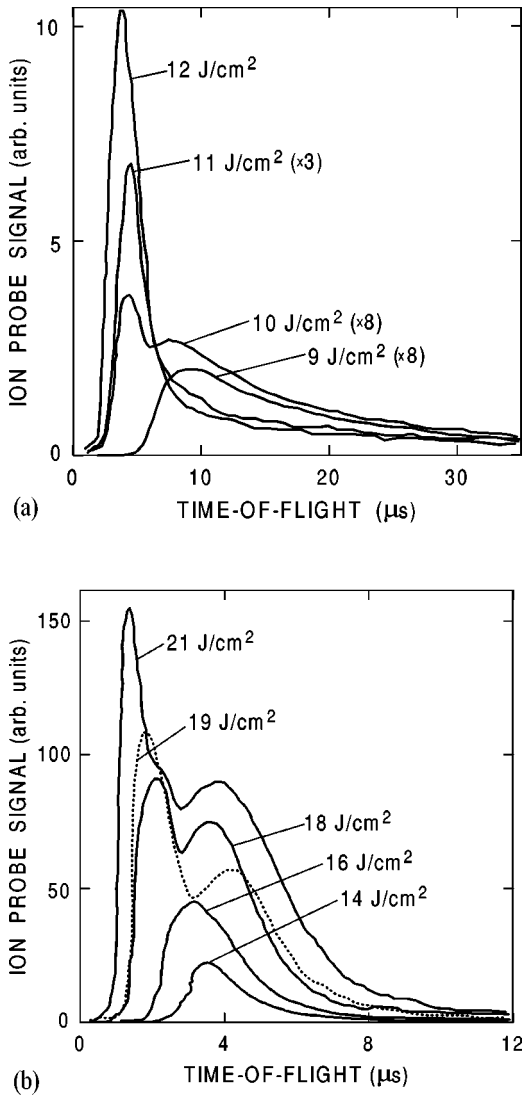

FIG. 3. As in Fig. 2 except that the target-to-collector distance is 89 mm.

increasing laser fluence for a target-to-collector distance of 89 mm is given in Fig. 3. At low laser fluence up to about 9 J/cm^2, the ion flux is weak and single-peaked. For a narrow fluence range, in the vicinity of 10 J/cm^2, the signal takes the double-peaked form, whereas at 11–16 J/cm^2 one can see only the fast peak whose arrival time decreases slowly with fluence. As the laser fluence increases further, the signal splits again into two components [see curves for 18, 19, and 21 J/cm^2 in Fig. 3(b)], so that the arrival time of the faster (''ultrafast'') component decreases drastically. This repeated splitting has not been observed at the target-to-collector distance of 30 mm (see in Fig. 2).

Figure 4 shows the average ion velocities calculated as the ratio of a target-to-collector distance to the peak time-of-flight as a function of laser fluence (for the double-peaked signal there are two average velocities for the fast and slow components). For 30 mm distance, after development of the fast component at 10 J/cm^2, the velocity of the slow component remains almost constant, nearly the same as that inherent in the single-peaked distribution at low laser fluence, up to about 13 J/cm^2 after which the slow peak is masked by the signal of the fast ions. For the target-to-collector dis-

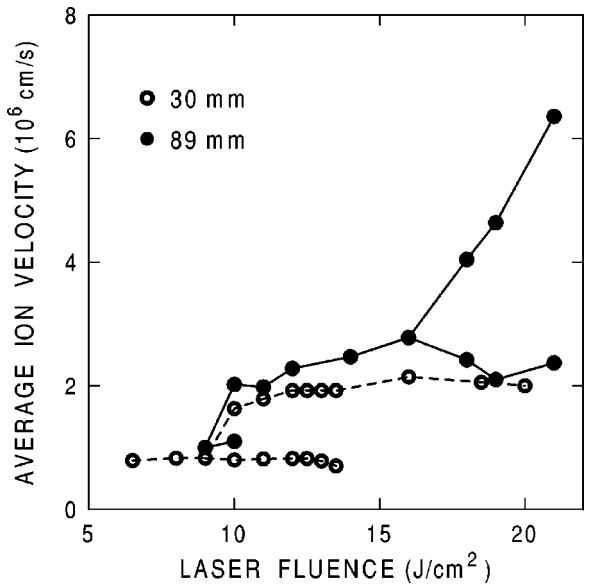

FIG. 4. Average velocity for each peak of ion TOF distributions, measured in vacuum at 30 mm (open points) and 89 mm (closed points) from the target, as a function of laser fluence at 1064 nm. For the double-peaked TOF signals there are two average velocities.

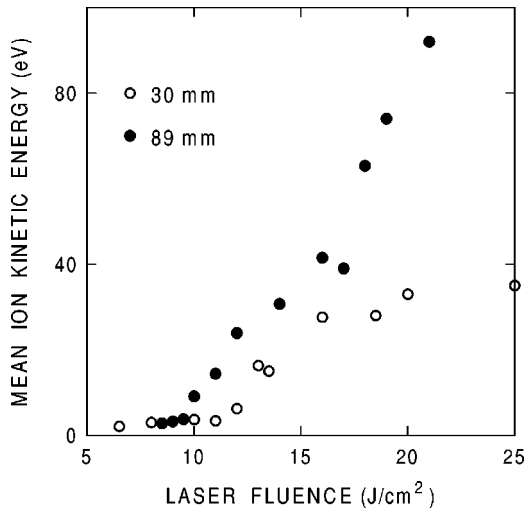

FIG. 5. Mean kinetic energy of ions $\langle E_{\mathrm{kin}}\rangle$ in vacuum at 30 mm (open points) and 89 mm (closed points) from the target as a function of laser fluence. The $\langle E_{\mathrm{kin}}\rangle$ values are calculated from the ion TOF distributions (Figs. 2 and 3) using Eq. (1).

tance of 89 mm, the picture is very similar up to fluence of 16 J/cm^2 when an ultrafast peak arises.

The mean kinetic energy gained per ion can be calculated from the TOF signal $I(t)$ as

$$\langle E_{\mathrm{kin}}\rangle = \frac{1}{2}\frac{\int_0^\infty m[u(t)]^2 I(t)dt}{\int_0^\infty I(t)dt} = \frac{mL^2}{2}\frac{\int_0^\infty t^{-2} I(t)dt}{\int_0^\infty I(t)dt}, \tag{1}$$

where m is the mass of the ion, $u(t)=L/t$ is the ion velocity, L is the target-to-collector distance. Equation (1) gives a tentative estimation since it assumes that only single charged atoms are present in the plume. In Fig. 5 the mean kinetic energies for each TOF spectrum (Figs. 2 and 3) are plotted against laser fluence. Equation (1) gives a tentative estimation since it assumes that only singly charged atoms are present in the plume. At high laser fluence, the calculated value of $\langle E_{\mathrm{kin}}\rangle$ is somewhat overestimated due to contributions to the signal of doubly charged ions (see analysis below). On the other hand, it is well known that carbon clusters are formed in abundance during laser ablation of graphite in vacuum [41–44] that implies an underestimation of the mean ion kinetic energy with Eq. (1). However, the contribution of the cluster ions is considerable at relatively low laser fluences, while at fluences important, as shown below, for the manifestation of the DL effects ($F_0 > 10$–12 J/cm^2 under the conditions considered), the ionized fraction of the plume is mainly formed by atomic carbon ions [22,41,42].

B. On the mechanisms of DL formation

Let us consider the peculiarities in signal behavior from the point of view of DL generation. First we evaluate the Debye length in the plume and its variation during plume expansion. To estimate the initial plume density, temperature and ionization degree, we assume (as in Ref. [17]) a uniform plasma cloud by the time the laser pulse has terminated. If the particle release from the surface is thermal in nature (that actually is the case with graphite for the studied ranges of laser fluences and wavelengths [45–47]), the cloud dimension along the target normal can be evaluated by $L_0 = u_t \tau$, where τ is the laser pulse duration and u_t is the thermal velocity of the particles defined by

$$u_t = \sqrt{\frac{8kT_s}{\pi m}} \tag{2}$$

with the surface temperature T_s. For fairly developed thermal ablation $T_s \approx 0.9\ T_c$ [48], where T_c is the thermodynamic critical temperature whose value for graphite is likely to be in the range of 12 000–15 000 K [46,49]. Taking $T_s = 12\,000$ K we obtain $L_0 \approx 0.06$ mm, a value substantially smaller than the irradiated spot radius $R_0 = 0.4$ mm. This implies that the plasma undergoes planar (i.e., one-dimensional) expansion during the laser pulse [36,37]. So, the initial density of the plume particles (atoms and ions) can be estimated as $n_0 = M/L_0 m$, where M is the target mass removed per pulse from a unit area. Measured values of M as a function of laser fluence are shown in Fig. 6(a). At fluences higher than ~ 10 J/cm^2, the ablated mass saturates at near 0.65 μg/(mm^2 pulse) and thus n_0 reaches its maximum value of about 5×10^{20} cm^{-3}. It should be noted that the measured target mass loss could differ from the actual ablation rate due to ejection of graphite particulates. It was found, however, that the particulate concentration in the plume is quite low for the most ablation regimes studied and appears not to affect the presented results significantly [21,46]. The situation is different for the high-fluence region ($F_0 > 20$ J/cm^2) when the explosive ablation mechanism dominates and the particulate fraction increases drastically [21,47].

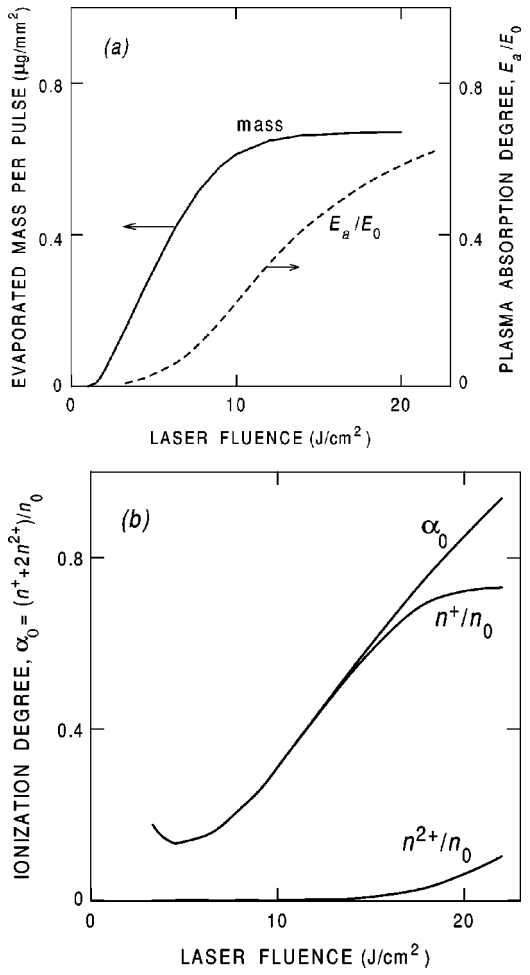

FIG. 6. (a) Target mass M, evaporated in vacuum per 1064-nm pulse from a unit surface area vs laser fluence (solid line represents the least square fit of the measured M values for different spot areas in the range 0.2–0.8 mm^2). Dashed line represents the data [46] on plasma absorption degree E_a/E_0. Here E_a is the energy absorbed by the plasma plume, E_0 is the incident laser energy. (b) Calculated values of the initial plasma ionization degree (at the end of the laser pulse) as a function of laser fluence. The lines labeled n^+/n_0 and n^{2+}/n_0 illustrate the contributions of singly and doubly charged carbon ions. Here n_0, n^+, and n^{2+} are the number densities of plume particles (atoms and ions), singly charged ions, and doubly charged ions, respectively.

To determine the initial plume temperature and the ionization degree, we considered the ionization balance for singly and doubly charged ions, taking into account the electron impact ionization, the photorecombination and the three-particle recombination. The source functions, written as in Ref. [50], were taken to be equal to zero under the assumption of a plasma in ionization equilibrium. Using an iterative procedure [17], the required parameters were calculated with known laser energy coupled to the plasma [see Fig. 6(a)]. In Fig. 6(b) the initial ionization degree α_0 and the fractions of the singly and doubly charged carbon atoms are presented as the functions of laser fluence. The doubly charged ions are predicted to be generated at $F_0 > 16$ J/cm^2 (the corresponding threshold intensity 1.2×10^9 W/cm^2 is in good agreement with the value measured in Ref. [51]) when the ultrafast peak in the TOF distribution is observed [Fig. 3(b)].

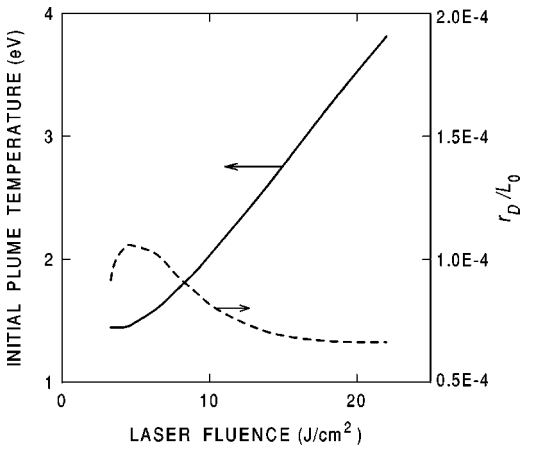

FIG. 7. Calculated values of initial plume temperature (solid line) and ratio of the Debye length to the plume axial dimension r_D/L_0, realized at the end of 13-ns laser pulse (dashed line), vs fluence for 1064-nm laser ablation of graphite in vacuum.

The calculated initial plume temperature (T_0) is plotted against laser fluence in Fig. 7 for the fluence range 6–25 J/cm^2 (or $0.5–2\times10^9$ W/cm^2). T_0 increases near linearly with fluence from $\sim$1.5 to 4 eV. These calculations are reasonably consistent with measurements [52] where the temperature of laser-generated carbon plasmas ($\sim$70 ns pulse) was found to vary in the range 2–8 eV for fluxes of 10^9–10^{10} W/cm^2. Knowing the initial plume parameters (n_0, T_0, α_0), we can estimate the Debye length of the plasma cloud by

$$r_D = \sqrt{\frac{kT_0}{8\pi e^2 n_e}},$$

where e is the electron charge, n_e is the initial electron density. The initial Debye length is about four orders of magnitude smaller than the axial cloud dimension throughout the considered fluence range (Fig. 7).

To evaluate the temporal evolution of the Debye length, we also performed calculations of carbon plasma expansion into vacuum using the spherical expansion model [17] with above initial plume parameters. The calculations have demonstrated that the ratio of the Debye length to the plume size increases only slightly during plasma expansion. This nontrivial fact can be understood from the following consideration. When the ionization degree of the plume is frozen out, the velocity of the expansion front reaches its maximum value given by [53]

$$u_f = \frac{2}{\gamma - 1} c_0.$$

Here $c_0 = (\gamma k T_0/m)^{1/2}$ is the initial speed of sound and γ is the specific heat ratio [for the considered temperature range (see Fig. 7) $\gamma = 1.2–1.3$ [53]]. Thereafter the expansion proceeds in a self-similar manner [54] and the plume dimension at the time moment t can be evaluated as $L_z = u_f t + L_0$. Assuming spherical adiabatic expansion, one can write that the average plume density, pressure and temperature decrease as $n \propto L_z^{-3}$, $p \propto L_z^{-3\gamma}$, and $T \propto L_z^{-3(\gamma-1)}$, respectively. Taking

$\gamma=1.25$, we have $r_D/L_z \propto (T/n)^{1/2}/L_z \propto L_z^{0.125} \propto t^{0.125}$. So, this simple consideration demonstrates that the r_D/L_z ratio has only a weak dependence on the expansion time.

Within a SET fluid approximation [26–28], the ambipolar electric field develops in a plasma boundary slab about the Debye length in thickness from where the electrons escape. The fraction of the ions accelerated by the ambipolar field can be estimated as $N_i^{\rm acc}/N_i = r_D/L_z$ [8], where $N_i^{\rm acc}$ is the number of the accelerated ions and N_i is the total number of the ions in the plume. As shown above, the calculated ratio r_D/L_z maintains its low value (10^{-3}–10^{-4}) during plasma expansion. In the range 10–20 J/cm^2, r_D/L_z varies within 20%, whereas the ion signal undergoes considerable transformation (see Fig. 2). This is difficult to explain in terms of SET fluid theory on the basis of the Debye length estimates.

Analyzing Figs. 2–7, one can point out the following.

(a) At low laser fluence, the mean kinetic energy of the ions (Fig. 5) is in agreement with the initial plume temperature T_0 estimated as 1.5–2.5 eV (Fig. 7). The rise in the mean kinetic energy of the ions much above T_0 is consistent with the formation of the well-developed double-peak structure at $F_0 \approx 10$–12 J/cm^2 (Figs. 2 and 3).

(b) Increase of the target-to-collector distance results in the formation of the double-peaked TOF distribution at lower F_0.

(c) The formation of an ultrafast ion peak at $F_0 > 16$ J/cm^2 is possibly due to the generation of doubly charged ions in the plume.

(d) At $F_0 < 10$ J/cm^2, the fraction of the accelerated ions is very small in accordance with the estimations of the Debye length.

The formation of the well-developed DL is therefore associated with the generation of hot (or tail) electrons which obtained additional energy in the expanding plume (for the other electrons the terms ''thermal'' and ''cold'' are commonly used). Two mechanisms may be responsible for the formation of hot electrons in laser-ablation plasmas: (a) three-body recombination when an electron is captured by an ion to some level (not to the ground state) with transfer of the excess energy to another electron [53] and (b) absorption of incident laser radiation due to inverse bremsstrahlung [5,29,31]. An argument in favor of the latter mechanism is the correlation between plasma absorption and ion acceleration [compare Figs. 4 and 6(a)].

What happens to the cold and hot electrons during the plume expansion? The rate of photorecombination depends on the electron temperature as $T_e^{-1/2}$, whereas the rate of three-body recombination follows a $T_e^{-9/2}$ dependence [53]. Thus, a cold electron has a large chance to recombine in collision with an ion, while a hot electron can take part in three-body recombination as a third particle, so that it gets additional energy becoming all the more energetic. The total cross section of the electron degradation in the gas phase tends to decrease with E_e at $E_e > 10$ eV [55]. Hence, the electrons that received an additional portion of energy are more capable of surviving compared to cold ones.

Let us follow the behavior of the DL on increasing the fraction of hot electrons based on Denavit's considerations [35]. In Fig. 8(a) a sketch of the DL structure is given for the case of a SET plasma. The plume consists of a quasineutral

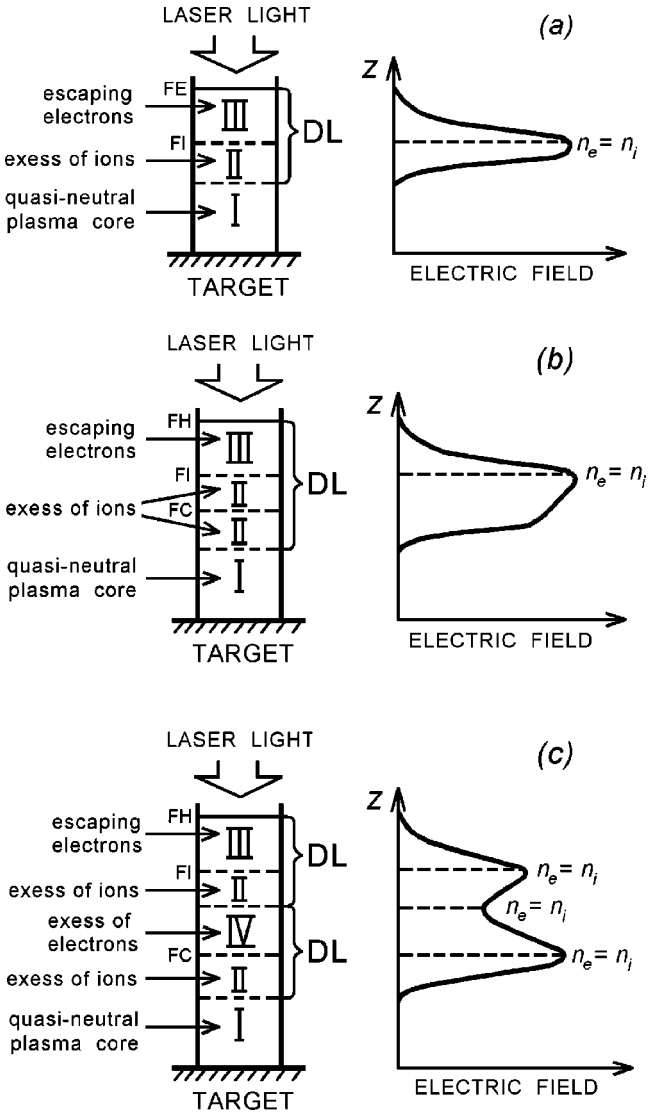

FIG. 8. Sketches in one dimension of the DL structures and profiles of ambipolar electric field for (a) SET plasma, (b) TET plasma with a small concentration of hot electrons, and (c) TET plasma when concentrations of hot and cold electrons are comparable (according to Denavit [35]). Here n_e and n_i are the number densities of electrons and ions. FE, FI, FH, and FC denote the front of electrons, ions, hot electrons, and cold electrons, respectively. For an explanation of the formation of regions I–IV in the plume see the text.

plasma core I, a region II of the order of r_D wide (up to the front of the ions FI) where quasineutrality breaks down, and a region III ahead of the plume where the electrons escape to. Under these conditions, a fraction of the ions thrown into region II, which is to say that they are involved in acceleration, is of the order of r_D/L_z. Of the same order is the width of the ambipolar electric field with the maximum located at $n_e = n_i$. With increasing laser fluence and the generation of a noticeable amount of hot electrons, the DL structure transforms to that shown in Figs. 8(b) and 8(c). For a relatively small ratio N_h/N_c ($\leqslant 10^{-2}$, N_h and N_c are the numbers of the hot and cold electrons in the plume), the peak of the ambipolar electric field is located close to FI, that is the boundary between the hot electrons and the ions involved

into acceleration, though the field gradient is maximized near the front of the cold electrons (FC) [Fig. 8(b)]. In addition, region II broadens resulting in more ions being accelerated as compared to the SET plasma. With further increasing laser fluence and associated increasing N_h/N_c ratio, a two-peak structure develops that can be recognized as two DLs with the peaks of the electric field located near FC (the inner DL) and FI [Fig. 8(c)]. The rise of the T_h/T_c ratio at a fixed N_h/N_c ratio leads to the same effect.

Mention should be made of the angular distributions of the plume ions. Upon integrating the TOF distributions (Figs. 2 and 3), we have obtained that the ion yield collected at 89 mm is less than that at 30 mm only by a factor of ~ 4 throughout the studied fluence range. If the angular distribution of ions follows a $\cos^p \theta$ dependence, θ being the angle with respect to the target normal, this corresponds to a very narrow distribution with $p \approx 60$. Similar strong forward peaking of the laser-produced ions ($p \approx 40$ assuming $\cos^p \theta$ approximation) was found using Langmuir probe [10]. Other observations demonstrate mush broader distributions approximated by $\cos^{(2n+1)} \theta$ dependences ($n = 1,2,3$) where n is the charge state of ions [56]. We attribute this discrepancy to the different plume geometry formed by the end of the laser pulse and thus to the different conditions for DL formation.

Generally, three types of initial conditions are possible, namely, $L_0 \ll R_0$, $L_0 \sim R_0$ and $L_0 \gg R_0$. Our view of the DL spatial structures for these three cases is illustrated in Fig. 9. At $L_0 \ll R_0$ (as is the case considered here), the DL develops at the early expansion stage and can be considered as planar [Fig. 9(a)]. In this case the ions subjected to the DL move into a narrow cone angle θ along the normal to the target. On further expansion, the accelerated ions have to maintain a near-planar DL structure while the main body of the plume loses the preferential pressure gradient and broadens considerably [57]. As a result, the accelerated ions move in a narrower cone angle than the slow ions and neutral particles. A similar tendency was observed in mass spectrometric measurements [16,58] where faster ions were found to have narrower angular distributions. For the case $L_0 \sim R_0$, the DL as well as the whole plume are shown to have nearly half-spherical symmetry [17,57] and the accelerated ions move in a wide angle [see Fig. 9(b)] as was probably the case in Ref. [56]. Finally, when the condition $L_0 \gg R_0$ is realized, the plume structure is reminiscent of a free gas jet issuing from a sonic nozzle, with its preferential motion in the forward direction since the late-vaporized particles act as a piston pushing the plume forward [Fig. 9(c)].

The mean kinetic energy of the ions obtained at 89 mm from the target is considerably higher than that at 30 mm for a given laser fluence $F_0 > 10$ J/cm^2 (Fig. 5). This fact can be explained by a number of reasons.

(a) The DL possibly does not degenerate by 30 mm but further accelerates the ions.

(b) A smaller fraction of the slow ions reaches the collector with increasing distance due to the broader angular distribution than that for the accelerated ions which escape from the same solid angle to a lesser extent.

(c) The time-average ion velocity $u = L/t$ used in Eq. (1) is clearly less than the true velocity at the collector position. This distinction is diminished with increasing distance.

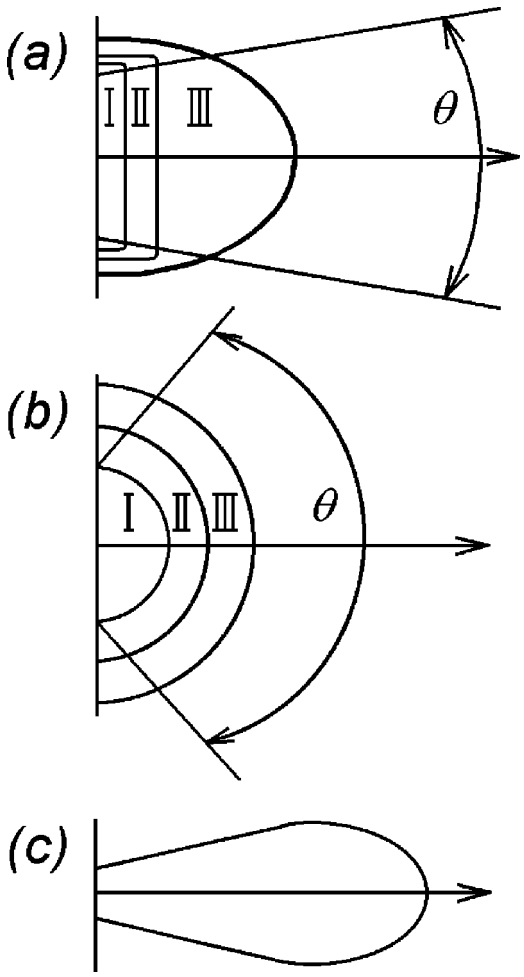

FIG. 9. Schematic representation of DL geometry for three types of initial conditions depending on the relationship between axial and transverse plume dimensions, L_0 and R_0, at the end of laser pulse: (a) $L_0 \ll R_0$, (b) $L_0 \sim R_0$, and (c) $L_0 \gg R_0$. The designations for the plume regions I–III are used as in Fig. 8. The region II with broken down quasineutrality can be separated by the region IV as in Fig. 8(c).

(d) The ion acceleration at fairly large distances can be caused by mechanisms other than the DL effects such as recombination and adiabatic expansion.

Only rough estimations of the contribution of each of the four listed factors can be made based on the present measurements. Obviously, velocity-dependent angular distributions play a role regardless of the collector position. Nevertheless, one can argue that the DL effect remains important beyond a 30-mm distance. This is supported by the dramatic increase in ion energy at $F_0 > 16$ J/cm^2 for 89 mm (Fig. 5). The doubly charged ions, to which we assign the ultrafast ion peak, experience twice as much acceleration in the ambipolar electric field as compared to singly charged ions. At 30 mm the doubly charged ions are not yet separated into an individual peak though they can already move in the front of the plume. The further free expansion and the action of the DL lead the doubly charged ions to be well ahead of the plume when detected at a greater distance. Factors (c) and (d) appear to be of minor importance since the main gas-dynamic acceleration and recombination energy release take place within a relatively small distance from the target under this ablation conditions [17].

C. On the approximation of ion TOF spectra by Maxwell-Boltzmann velocity distributions

Many ion-probe measurements performed under PLD conditions demonstrate that the TOF signal can be fitted by a Maxwell-Boltzmann distribution superimposed on a flow velocity (so-called shifted Maxwellian) [22,39,59–61]. Such a distribution is similar to that realized in an adiabatic supersonic expansion of gaseous jets and is believed to be established due to collisions of the ablated particles in a near-surface region termed the Knudsen layer [37,62]. A good fit of the measured spectra by a shifted Maxwellian is often interpreted as indication that the thermalization of the plume particles occurs and therefore the flow velocity and effective plume temperature can be deduced from the fit. On the other hand, such an approximation, when applied to the ions subjected to the DL, appears to have no physical ground since the velocities of the accelerated ions are driven mainly by the ambipolar electric field and are not representative of the plasma bulk expansion. One can expect therefore that the approximation of the TOF distributions by Maxwell-Boltzmann functions (and needless to say by their superposition) will result in meaningless fitting parameters if the accelerated ions contribute significantly to the measured signal.

To demonstrate this, we have performed fitting of the TOF spectra (single-peaked distributions from Figs. 2 and 3) with a shifted Maxwellian which is given for our flux-sensitive detector by [62]

$$I(t)=At^{-5}\exp\left[-\frac{m(L/t-u_f)^2}{2kT_{\mathrm{eff}}}\right], \tag{3}$$

where A is a normalization constant, u_f is the flow velocity, and T_{eff} is the effective temperature associated with translational motion along the plume axis. Figure 10 shows representative TOF data and corresponding fits. At low laser fluence (~ 8 J/cm^2), when no essential DL effect occurs, the signal can be poorly described by a Maxwellian because of a low-velocity non-Maxwellian tail in the distribution [Fig. 10(a)]. The latter is most likely due to the carbon cluster ions which are formed in abundance during 1064 nm laser ablation of graphite at moderate fluences [41,44]. Nevertheless, the fitting parameters are quite reasonable for an adiabatic expansion. T_{eff} is less than the initial plume temperature estimated as $T_0 \approx 20\,000$ K for 8 J/cm^2 (see Fig. 7). Also, the flow velocity of ~ 5.9 km/s is in a comparable range with the value $u_f \sim (kT_0/m)^{1/2} \approx 4$ km/s expected downstream of the Knudsen layer [37].

The agreement between the measured TOF distributions and the fits with Eq. (3) seems at first sight to be much better for 16 J/cm^2 [Figs. 10(b) and 10(c)], a fluence where the accelerated ions contribute significantly to the signal (see Sec. III B). However, the obtained fitting parameters appear to be unreasonably high taking into account that $T_0 \approx 30\,000$ K (Fig. 7). Moreover, T_{eff} increases with distance which cannot be explained by assuming a collision-driven supersonic expansion. Therefore, when using a Maxwellian fit of the ion TOF spectrum for a laser-produced plasma, some care is needed. In our view, this situation is similar to that for photochemical desorption when nonthermally desorbed molecules have formally a Maxwell-Boltzmann velocity distribution without any thermalization [63].

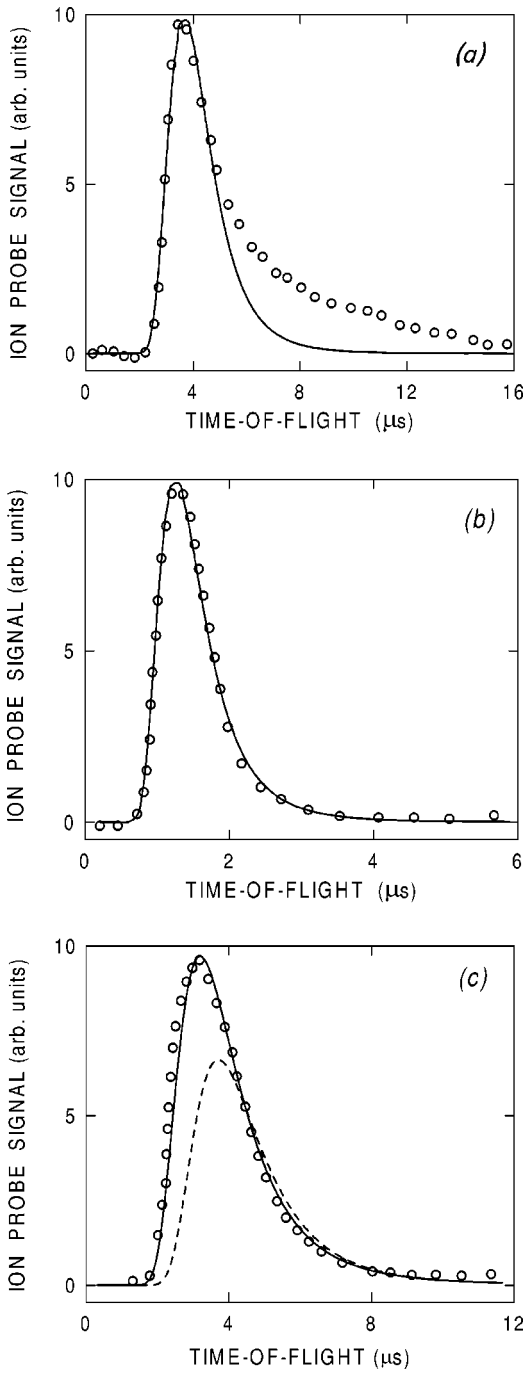

FIG. 10. Representative ion TOF spectra obtained in vacuum at 1064-nm laser wavelength (points) and corresponding fits with a Maxwell-Boltzmann distribution [Eq. (3), solid lines]. (a) Laser fluence $F_0 = 8$ J/cm^2, target-to-collector distance $L = 30$ mm; fitting parameters in Eq. (3) are $T_{\mathrm{eff}} = 5500$ K, $u_f = 5.94$ km/s. (b) $F_0 = 16$ J/cm^2, $L = 30$ mm, $T_{\mathrm{eff}} = 75\,000$ K, $u_f = 13$ km/s. (c) $F_0 = 16$ J/cm^2, $L = 89$ mm, $T_{\mathrm{eff}} = 140\,000$ K, $u_f = 11$ km/s. Dashed line in (c), being the same as solid line in (b), illustrates the changes in ion TOF distribution with increasing distance from the target.

D. Effect of radiation wavelength

For most materials, the threshold fluence for ablation is lower for shorter wavelengths due to the higher absorption

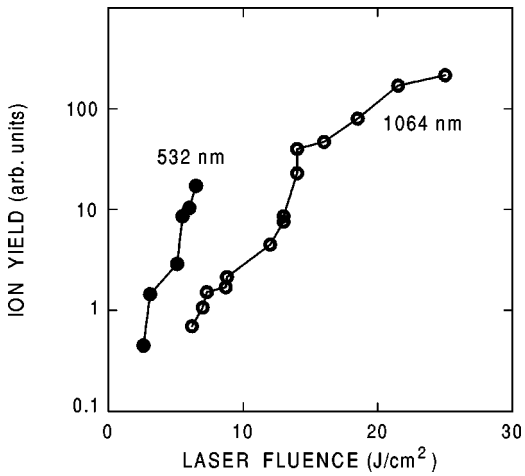

FIG. 11. Ion yield obtained by integrating the TOF distributions collected in vacuum at 30 mm from the target as a function of laser fluence at 1064 nm (open points) and 532 nm (closed points).

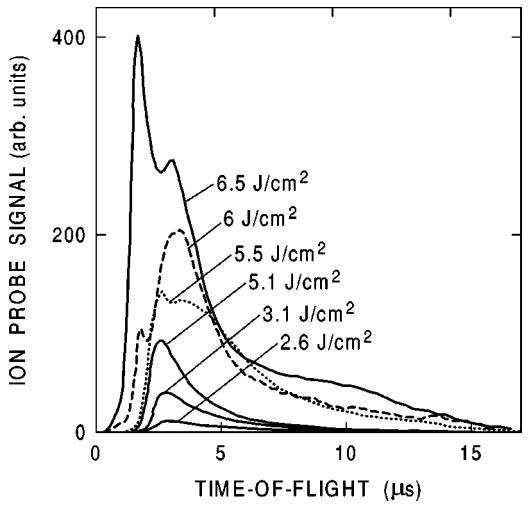

FIG. 12. Ion TOF distributions in vacuum for different laser fluences at 532-nm wavelength. The target-to-collector distance is 30 mm.

coefficients, but the ablation depth increases with fluence more rapidly for longer wavelength (see, e.g., Ref. [64]). This effect may be partly obscured by efficient heat conduction process in the graphite target. It should be noted, however, that the role of thermal conductivity becomes less significant with increasing temperature [thermal diffusion length $l_{\mathrm{th}}=(k\tau/c\rho)^{1/2}=1300$ nm at 300 K and 270 nm at 3000 K, where τ is the laser pulse duration, k is the thermal conductivity, c is the specific heat and ρ is the mass density; the values of graphite properties are taken from Refs. [65,66]]. The wavelength effect is therefore quite prominent under the considered conditions of relatively high fluences. In particular, at ~ 6 J/cm^2, the ablation depth of graphite measured for 532-nm laser radiation (the optical penetration depth $d\approx 30$ nm [67]) is about 1.7 times smaller than that at 1064 nm ($d\approx 67$ nm [67]). This means that nearly the same amount of laser energy is coupled to the lower number of particles resulting obviously in higher initial plume temperatures and thus in higher ionization degrees. Indeed, our ion-probe experiments demonstrate that, for fixed laser fluence, the ions are much more abundant in the plume at 532 nm than at 1064 nm. The ion yields obtained by integrating the measured TOF distributions are shown in Fig. 11 for both wavelengths. At 1064 nm, the observed threshold for ion appearance is only slightly lower than the maximum fluence of 6.5 J/cm^2 obtained with the 532-nm radiation. At this fluence, the collected ion yields differ more than by order of magnitude.

Figure 12 shows the ion-probe signals obtained on irradiation of the graphite target with 532-nm laser light. The qualitative behavior of the signal with increasing laser fluence is similar to that obtained in the 1064-nm experiments. The most probable ion velocities at 2.6–5.5 J/cm^2 (when single-peak distributions are observed) are, however, somewhat higher than those at 1064 nm (see curves for 6.5 and 8 J/cm^2 in Fig. 2). Along with the early appearance of the ions, it confirms the higher initial temperature of the plume. On the other hand, the accelerated ions have nearly the same most probable velocity for both wavelengths [compare curves at 6 and 6.5 J/cm^2 in Fig. 12 and at 12 and 13 J/cm^2 in Fig. 2(b)].

E. Effect of background gas

The pressure of the background gas is one of the key parameters in PLD. Increasing the background pressure has been shown to cause splitting of the plume ions into a fast and slow component [11,12]. The phenomenon of plume splitting has been described with model calculations in terms of the scattering dynamics of the plume particles on the background molecules [12]. In Ref. [14], where the ion-probe signal was measured at rather small target-to-collector distances in the background gas, the transformation of the double-peaked structure into a single-peaked structure was observed with increasing detection distance. It was also found that the average velocity of the ion flux decreases with the background pressure. The oscillatory behavior of a plume in an ambient gas resulting in multipeak TOF distributions has been described using the hydrodynamic models [17,57]. It is of interest to examine how the pressure of background gas influences the ion kinetic energies under PLD conditions, taking into account that the ions can be subjected to acceleration in the DL.

Figure 13 shows the influence of the air pressure on TOF distribution at 25 J/cm^2 and 1064-nm wavelength. When the collector was located at 30 mm from the target, the single-peaked structure was observed up to a pressure of about 3 Pa [Fig. 13(a)]. At ~ 5 Pa, one can see the appearance of a weak peak of the slow ions (shown by arrow). On further increase of the background pressure, the arrival time of the fast peak decreases, while that of the slow ions increases. At 89 mm from the target, the slow ion peak has not been observed up to ~ 7 Pa, whereas at higher pressure the ions were not detectable [Fig. 13(b)].

The peak arrival time and the mean kinetic energy of the ions derived from Fig. 13 are shown in Fig. 14 as a function of the background pressure. There are two intriguing features: (a) There is an apparent decrease of the arrival time of the fast ion peak with pressure. A similar effect was observed at smaller target-to-collector distances [14]. (b) The mean kinetic energy of the ions increases with the background pressure at 89 mm, while decreases at 30 mm.

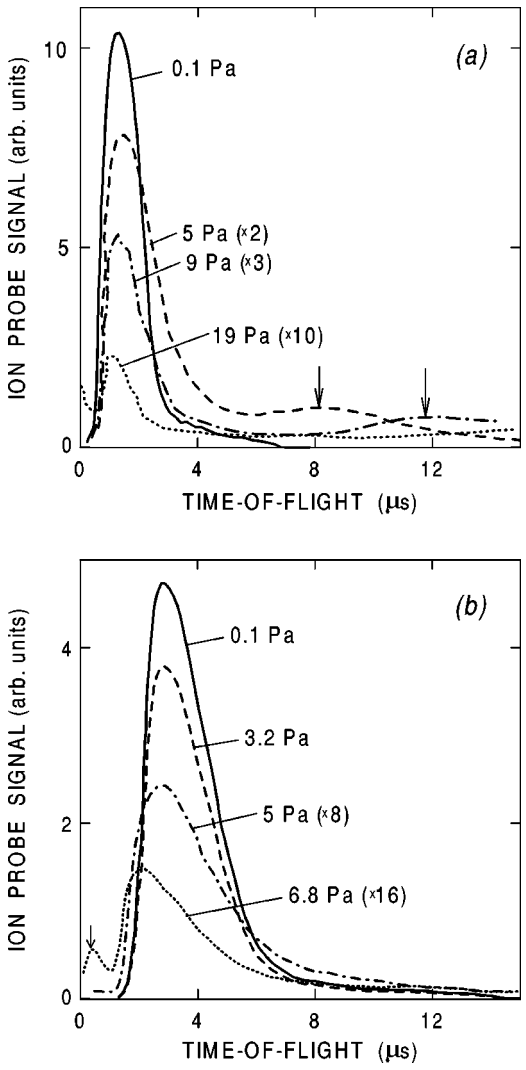

FIG. 13. Ion TOF distributions measured at 30 mm (a) and 89 mm (b) from the target at various background air pressures. Laser fluence is 25 J/cm^2 at 1064 nm. The arrows in (a) show the peaks of slow ions at background pressures of 5 and 9 Pa (at 19 Pa the flux of slow ions peaks at 19.5 ms). The arrow in (b) shows the peak arising due to ionization of the background gas.

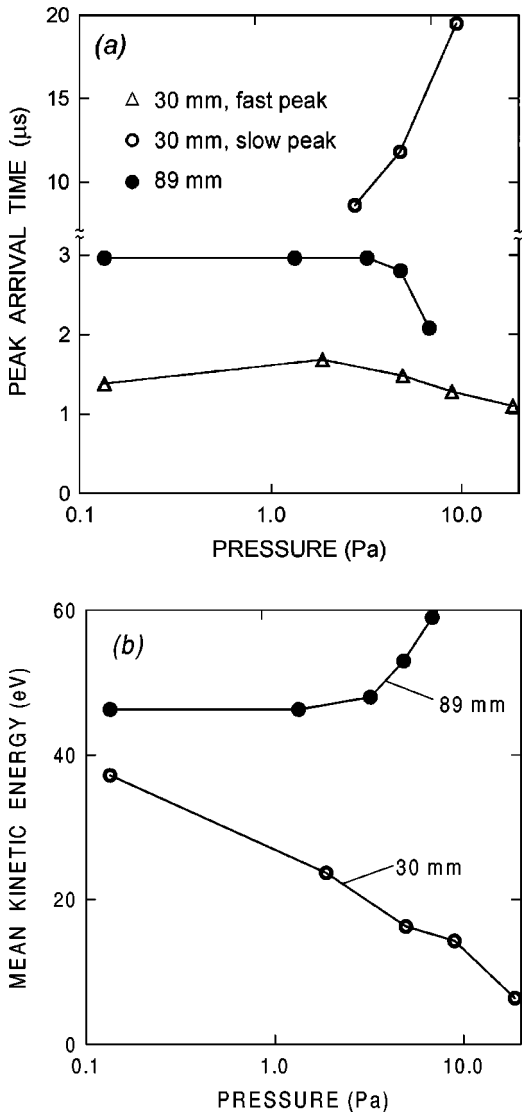

FIG. 14. The most probable arrival time of fast and slow ions (a) and mean kinetic energy of the ions $\langle E_{\mathrm{kin}} \rangle$, vs background gas pressure. The data are derived from the TOF spectra shown in Figs. 13(a) and 13(b). The $\langle E_{\mathrm{kin}} \rangle$ values are calculated using Eq. (1).

In the presence of background gas, the effect of DL formation is superimposed on scattering of the plume particles. As the absorption of laser radiation by the plume is considerable in the fluence range studied (see Fig. 6), a high-energetic electron tail is generated that leads to the developed DL as shown in Figs. 8(b) or 8(c). The ions accelerated in the DL are scattered by the background gas to a lesser extent on their way to the collector since the total scattering cross-section decreases with ion energy [55]. As a result, only the faster part of the ions reaches a distant collector. Obviously this part decreases with increasing background pressure until the ion flux degradates. Though the DL becomes weaker due to a decreased number of ions, it continues to accelerate the front ions thus enhancing their kinetic energy. Depending on the relation between ion acceleration in the ambipolar electric field and scattering of ions by the background gas, the arrival time of the fast ion peak can decrease or increase. This is a subject of further study. Evidently, the mentioned relation varies with the distance from the target. An additional peak at 6.8 Pa with a short arrival time [shown by the arrow in Fig. 13(b)] originates presumably from the background molecules ionized in the immediate vicinity of the collector by the plume electrons. Clearly, it should not be considered when evaluating the mean kinetic energy of the ions.

The part of the ions, being scattered and thermalized, forms the second (slow) peak which is observed at small distance and becomes undetectable at 89 mm. Depending on the background pressure, two main mechanisms can be responsible for it. (1) The slow ions flux is attenuated by the background gas to a greater extent than that of fast ions [55]. (2) The formation of the hydrodynamic regime of the plume flow with increasing background pressure leads to ''locking up'' of the slow ions by the plume. Consider the second effect in more detail. At low background pressure, the plume core almost does not feel the counteraction of the background gas whereas the fast ion flux is exponentially attenuated with distance and pressure [11]. As the background

pressure increases, the ambient gas begins to brake the expansion of the plume, while the plume, acting as a piston, snowploughs the background gas. As a result, the hydrodynamic regime of plume expansion is formed with the generation of a shock wave structure. The details of such a regime are described in Refs. [17,57]. The high-energetic ions, formed at an early stage of the plume expansion, penetrate deeply into the background gas and reach a distant collector. The slower ions move together with the main body of the plume. The plume expanding into a background gas propagates to a finite distance from the target that decreases with gas pressure [17,57]. At fairly high background pressure the plume propagation length becomes less than the target-to-collector distance. When this takes place, plume particles other than the high-energetic ions reach the collector through diffusion in the background gas. In doing so, the thermalized ions experience recombination, so that the slow-ion peak disappears.

When increasing the background pressure, we observed, apart of the appearance of the slow ion peak for the originally single-peaked ion current (as in Ref. [11]), the transformation of the double-peaked structure into the single-peaked signal of the slow ions only. The described effect calls for further investigations.

IV. CONCLUSIONS

In summary, the ion probe technique has been used for the detailed study of ion expansion during laser ablation of graphite in a laser fluence range important for PLD. From the results and the discussion, the following conclusions can be made.

(1) The appearance of a double-peaked structure in the ion TOF distribution both under vacuum and in background gas is explained by the formation of an ambipolar electric field (double layer) in the expanding plume.

(2) The observed ion acceleration can not be ascribed to breaking quasineutrality in the plume boundary over the Debye length in the single-electron-temperature fluid approach. To account for the detected kinetic energies of the ions, the generation of a high-energetic electron tail due to absorption of laser radiation in the plume has to be considered. The appearance of an ultrafast peak in the TOF distribution correlates with the formation of doubly charged ions in noticeable amounts.

(3) The ions accelerated in the DL should have most probably non-Maxwellian velocity distributions. If the accelerated ions contribute significantly to the signal, the approximation of the ion TOF spectrum by a Maxwellian results in meaningless fitting parameters.

(4) At 532-nm ablation, the DL effect becomes significant at a lower laser fluence than at 1064-nm irradiation due to the higher ion yield at shorter wavelengths.

(5) The background gas depresses the DL effect. The time-of-flight of the fast-ion peak can decrease or increase with increasing background pressure depending on the relation between ion scattering by the background molecules and ion acceleration by the ambipolar electric field. This relation varies with the distance from the target.

We suppose that the DL effects considered in this paper are more general and play a role in PLD of various materials. Our preliminary results of ion-probe measurements on the ablation products from Si and Nb targets have shown quite similar behavior of the ion-collector signal as that described above. It seems that there is much scope for further study as understanding of ion acceleration in detail can lead to better optimization of the PLD process.

ACKNOWLEDGMENTS

We are deeply indebted to Eleanor E. B. Campbell for her interest and her helpful and critical remarks on this investigation. The work was supported by the Russian Foundation for Basic Research (Grants Nos. 97-02-18489 and 99-03-32331) and by the Russian Scientific Program ''Fullerenes and Atomic Clusters'' (Project No. 5-4-99).

[1] A. A. Plyutto, Zh. Éksp. Teor. Fiz. **39**, 1589 (1960) [Sov. Phys. JETP **12**, 1106 (1961)].
[2] G. Hairapetian and R. L. Stenzel, Phys. Fluids B **3**, 899 (1991).
[3] K. Dick, H. Pépin, J. Martineau, K. Parbhakar, and A. Thibaudeau, J. Appl. Phys. **44**, 3284 (1973).
[4] P. E. Dyer, S. A. Ramsden, J. A. Sayers, and M. A. Skipper, J. Phys. D **9**, 373 (1976).
[5] J. S. Pearlman, J. J. Thomson, and C. E. Max, Phys. Rev. Lett. **38**, 1397 (1977).
[6] P. Wägli and T. P. Donaldson, Phys. Rev. Lett. **40**, 875 (1978).
[7] R. Decoste and B. H. Ripin, Phys. Rev. Lett. **40**, 34 (1978).
[8] Yu. A. Bykovsky, V. G. Degtyarev, N. N. Degtyarenko, V. F. Elesin, I. D. Laptev, and V. N. Nevolin, Zh. Tech. Fiz. **42**, 658 (1972) [Sov. Phys. Tech. Phys. **17**, 380 (1972)].
[9] W. Demtröder and W. Jantz, Plasma Phys. **12**, 691 (1970).
[10] R. J. von Gutfeld and R. W. Dreyfus, Appl. Phys. Lett. **54**, 1212 (1989).
[11] D. B. Geohegan and A. A. Puretzky, Appl. Surf. Sci. **96-98**, 131 (1996).
[12] R. F. Wood, J. N. Leboeuf, D. B. Geohegan, A. A. Puretzky, and K. R. Chen, Phys. Rev. B **58**, 1533 (1998).
[13] S. Metev, M. Ozegowski, G. Sepold, and S. Burmester, Appl. Surf. Sci. **96-98**, 122 (1996).
[14] J. Brčka, M. Alunovic, A. Voss, and E. W. Kreutz, Plasma Sources Sci. Technol. **3**, 128 (1994).
[15] K. Fukushima, Y. Kanke, M. Badaye, and T. Morishita, J. Appl. Phys. **77**, 5404 (1995).
[16] G. Ulmer, B. Hasselberger, H.-G. Busmann, and E. E. B. Campbell, Appl. Surf. Sci. **46**, 272 (1990).
[17] A. V. Bulgakov and N. M. Bulgakova, J. Phys. D **28**, 1710 (1995).
[18] X. D. Wu, A. Inam, T. Venkatesan, C. C. Chang, E. W. Chase, P. Barboux, J. M. Tarascon, and B. Wilkens, Appl. Phys. Lett. **52**, 754 (1988).
[19] H. Izumi, K. Ohata, T. Hase, K. Suzuki, T. Morishita, and S. Tanaka, J. Appl. Phys. **68**, 6331 (1990).
[20] J. J. Cuomo, D. L. Pappas, J. Bruley, J. P. Doyle, and K. L. Saenger, J. Appl. Phys. **70**, 1706 (1991).
[21] C. W. Ong, X.-A. Zhao, J. T. Cheung, S. K. Lam, P. W. Chan, and C. L. Choy, Appl. Phys. A: Mater. Sci. Process **63**, 287

(1996).
[22] J. Dias, S. Ferrer, and F. Comin, J. Appl. Phys. **84**, 572 (1998).
[23] R. Jordan, D. Cole, J. G. Lunney, K. Mackay, and D. Givord, Appl. Surf. Sci. **86**, 24 (1995).
[24] M. Tanaka, Y. Fujisawa, T. Nakajima, and Y. Tasaka, J. Appl. Phys. **83**, 3379 (1998).
[25] A. J. Peurrung, J. P. Cowin, G. Teeter, S. E. Barlow, and T. M. Orlando, J. Appl. Phys. **78**, 481 (1995).
[26] M. Widner, I. Alexeff, and W. D. Jones, Phys. Fluids **14**, 695 (1971).
[27] J. E. Crow, P. L. Auer, and J. E. Allen, Plasma Phys. **14**, 65 (1975).
[28] A. V. Gurevich and W. P. Meshcherkin, Zh. Éksp. Teor. Fiz. **80**, 1810 (1981) [Sov. Phys. JETP **53**, 937 (1981)].
[29] B. Bezzerides, D. W. Forslund, and E. L. Lindman, Phys. Fluids **231**, 2179 (1978).
[30] L. M. Wickens, J. E. Allen, and P. T. Rumsby, Phys. Rev. Lett. **41**, 243 (1978).
[31] R. L. Morse and C. W. Nielson, Phys. Fluids **16**, 909 (1973).
[32] M. A. True, J. R. Albritton, and E. A. Williams, Phys. Fluids **24**, 1885 (1981).
[33] L. M. Wickens and J. E. Allen, Phys. Fluids **24**, 1894 (1981).
[34] S. J. Gitomer, R. D. Jones, F. Begay, A. W. Ehler, J. F. Kephart, and R. Kristal, Phys. Fluids **29**, 2679 (1986).
[35] J. Denavit, Phys. Fluids **22**, 1384 (1979).
[36] R. K. Singh and J. Narayan, Phys. Rev. B **41**, 8843 (1990).
[37] R. Kelly, Phys. Rev. A **46**, 860 (1992).
[38] J. S. Pearlman, Rev. Sci. Instrum. **48**, 1064 (1977).
[39] S. Amoruso, M. Armenente, R. Bruzzese, and N. Spinelli, Appl. Phys. A: Mater Sci. Process. **65**, 265 (1997).
[40] D. L. Pappas, K. L. Saenger, J. J. Guomo, and R. W. Dreyfuss, J. Appl. Phys. **72**, 3966 (1992).
[41] G. Seifert, S. Becker, and H.-J. Dietze, Int. J. Mass Spectrom. Ion Processes **84**, 121 (1988).
[42] J. J. Gaumet, A. Wakisaka, Y. Shimizu, and Y. Tamori, J. Chem. Soc., Faraday Trans. **89**, 1667 (1993).
[43] D. J. Krajnovich, J. Chem. Phys. **102**, 726 (1995).
[44] B. N. Kozlov, S. N. Kirillov, and B. A. Mamyrin, Proc. SPIE **3093**, 233 (1997).
[45] R. W. Dreyfuss, R. Kelly, and R. E. Walkup, Nucl. Instrum. Methods Phys. Res. B **23**, 557 (1987).
[46] A. V. Bulgakov and N. M. Bulgakova, Kvantovaya Elektronika **27**, 154 (1999) [Quantum Electron. **29**, 154 (1999)].
[47] N. M. Bulgakova and A. V. Bulgakov, Appl. Phys. A: Mater. Sci. Process. (to be published).
[48] R. Kelly and A. Miotello, Nucl. Instrum. Methods Phys. Res. B **122**, 374 (1997).
[49] M. M. Martynyuk, Zh. Fiz. Khimii **57**, 810 (1983) [Russ. J. Phys. Chem. **57**, 494 (1983)].
[50] E. E. Lovetsky, A. N. Polianitshev, and V. S. Fetisov, Fizika Plasmy **1**, 773 (1975) [Sov. J. Plasma Phys. **1**, 422 (1975)].
[51] P. Langer, G. Tonon, F. Floux, and A. Ducauze, J. Quantum Electron. **2**, 499 (1966).
[52] C. D. David, Jr. and H. Weichel, J. Appl. Phys. **40**, 3674 (1969).
[53] Ya. B. Zeldovich and Yu. P. Raizer, *Physics of Shock Waves and High-Temperature Hydrodynamic Phenomena* (Academic Press, New York, 1996).
[54] L. I. Sedov, *Similarity and Dimensional Methods in Mechanics* (Cleaver Hume, London, 1959).
[55] M. Kimura, M. Inokuti, and M. A. Dillon, Adv. Chem. Phys. **84**, 193 (1993).
[56] K. Mann and K. Rohr, Laser Part. Beams **10**, 435 (1992).
[57] A. V. Bulgakov and N. M. Bulgakova, J. Phys. D **31**, 693 (1998).
[58] Yu. A. Bykovsky, N. N. Degtyarenko, V. F. Yelesin, Yu. P. Kozyrev, and S. M. Silnov, Zh. Éksp. Teor. Fiz. **60**, 1306 (1971) [Sov. Phys. JETP **33**, 783 (1972)].
[59] J. P. Zheng, Z. Q. Huang, D. T. Shaw, and H. S. Kwok, Appl. Phys. Lett. **54**, 280 (1989).
[60] K. Fukusima, Y. Kanke, and T. Morishita, J. Appl. Phys. **74**, 6948 (1993).
[61] K. J. Koivisaari, J. Levoska, and S. Leppävuori, J. Appl. Phys. **85**, 2915 (1999).
[62] R. Kelly and R. W. Dreyfus, Surf. Sci. **198**, 263 (1988).
[63] F. M. Zimmermann and W. Ho, J. Chem. Phys. **100**, 7700 (1994).
[64] J. Heitz, J. D. Pedarnig, D. Bäuerle, and G. Petzow, Appl. Phys. A: Mater. Sci. Process. **65**, 259 (1997).
[65] *Handbook of Physical Quantities*, edited by I. S. Grigoriev and E. Z. Meilikhov (CRC Press, Boca Raton, 1995).
[66] *Handbook of Thermal Conductivity of Solids*, edited by A. S. Okhotin (Energoatomizdat, Moscow, 1984) (in Russian).
[67] V. M. Zolotarev, V. N. Morozov, and E. V. Smirnova, *Optical Constants for Natural and Technical Media* (Khimia, Leningrad, 1984), in Russian.